THE JOURNAL OF PHYSICAL CHEMISTRY B

Article

pubs.acs.org/JPCB

Stochastic Modeling of Flexible Biomolecules Applied to NMR Relaxation. 2. Interpretation of Complex Dynamics in Linear Oligosaccharides

Dmytro Kotsyubynskyy,[†] Mirco Zerbetto,[†] Maria Soltesova,[‡,∥] Olof Engström,[§] Robert Pendrill,[§] Jozef Kowalewski,[‡] Göran Widmalm,[§] and Antonino Polimeno*,[†]

[†]Dipartimento di Scienze Chimiche, Università degli Studi di Padova, Padova 35131, Italy

[‡]Department of Materials and Environmental Chemistry, and [§]Department of Organic Chemistry, Stockholm University, S-106 91 Stockholm, Sweden

[∥]Department of Low Temperature Physics, Faculty of Mathematics and Physics, Charles University in Prague, Czech Republic

Supporting Information

ABSTRACT: A computational stochastic approach is applied to the description of flexible molecules. By combining (i) molecular dynamics simulations, (ii) hydrodynamics approaches, and (iii) a multidimensional diffusive description for internal and global dynamics, it is possible to build an efficient integrated approach to the interpretation of relaxation processes in flexible systems. In particular, the model is applied to the interpretation of nuclear magnetic relaxation measurements of linear oligosaccharides, namely a mannose-containing trisaccharide and the pentasaccharide LNF-1. Experimental data are reproduced with sufficient accuracy without free model parameters.

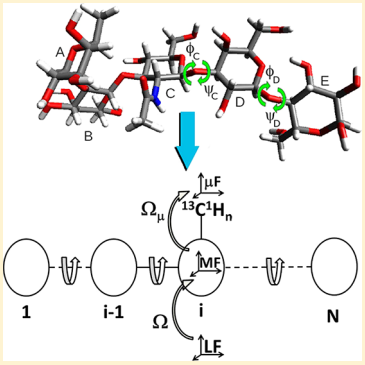

I. INTRODUCTION

Recently, the combination of stochastic modeling of relevant molecular coordinates with ad hoc computational tools for the evaluations of molecular properties was shown in several instances to be an effective approach for the calculation of spectroscopic observables, related to relaxation processes of complex molecular systems in condensed phase.[1−4] Stochastic approaches, which are based on the assumption that a reduced set of coordinates can be described as a Markov process by a suitably defined Fokker−Planck equation, are interesting tools, especially when applied in the field of computational spectroscopy. They allow relatively computationally inexpensive ways to interpret observables characterized by a vast range of relaxation rates, and they can be easily merged with other computational tools to evaluate parameters otherwise obtainable only via fitting procedures.

In the past, two main phenomenological approaches have settled in the scene of the interpretation of NMR data. The former is the time honored model free (MF) approach of Lipari and Szabo,[5] and the second is the slowly relaxing local structure (SLRS) model of Polimeno and Freed.[6−8] Formally, both approaches are two-body phenomenological models based on the interpretation of the dynamics of the molecule as the combination of a global tumbling motion and the local confined rotational motion of a reference frame fixed on the magnetic probe, collecting the internal motions of the molecule. The two main differences between the MF and the SRLS approaches are: (i) MF is based on the statistical independence of the two rotational motions, whereas SRLS exactly accounts for coupling when it is necessary and (ii) local geometries (tilt angles between different magnetic interactions) are not taken into account in MF, whereas they are part of the set of parameters used in defining the SRLS model. Usually a two- or three-exponential correlation function is more than sufficient to well fit experimental NMR data, making it difficult to establish which model is the more performing in terms of agreement with experiments. The point to be discussed is the information provided by the model parameters. In both cases one can recover information on restrictions to the local motion and about its correlation time. However, the physical picture is usually so complex that it cannot always be calculated. This means that a multicomponent fitting procedure is usually required to access the model parameters with all the problems related to fitting, i.e., (i) it is commonly found that the number of available experimental data is smaller (or in the same order) of the model parameters; (ii) the χ^2 surface on the model parameters space may present multiple relative minima that poses serious complications on the search of the best set of

Received: July 4, 2012
Revised: November 13, 2012
Published: November 27, 2012

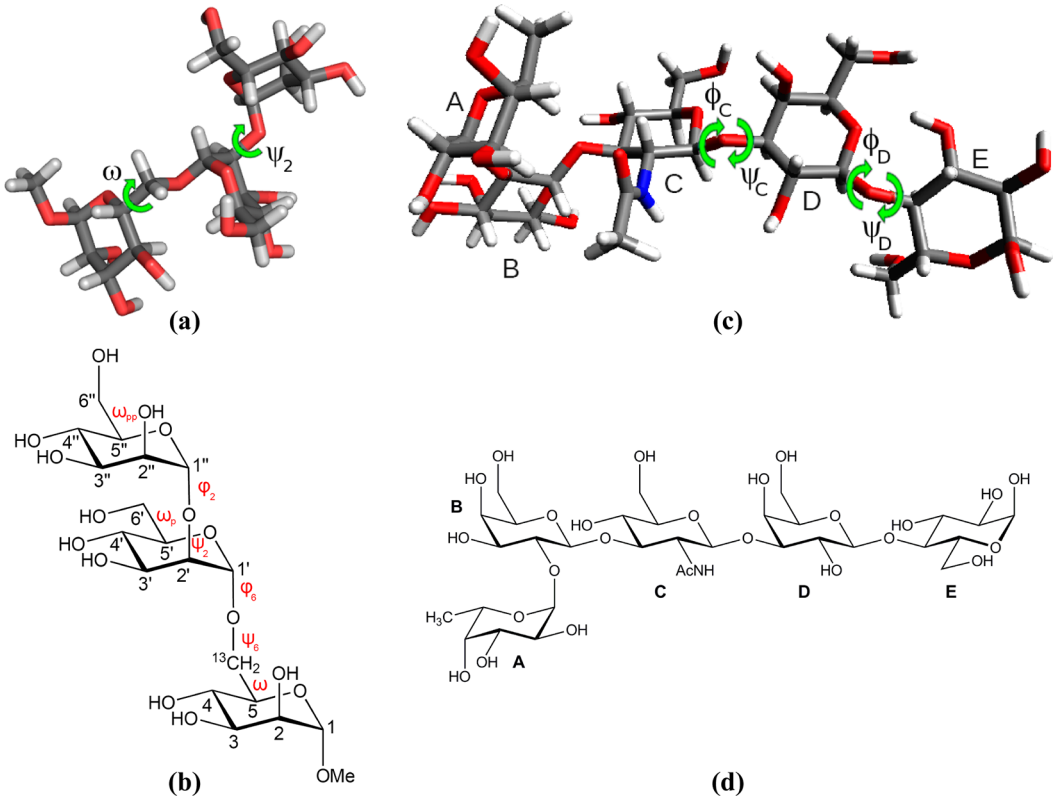

Figure 1. (a) Sticks model representation and (b) schematic of trisaccharide **TRI** molecule; (c) sticks model representation and (d) schematic of pentasaccharide **LNF-1** molecule (sugar residues are labeled with capital Latin letters). Torsion angles that we considered as relevant in the DCM analysis of NMR data are highlighted in panels a and c.

model parameters that should fulfill both the requirements of good agreement with experiment and their physical (presumed) correctness; (iii) force fitting may be encountered when a too small number of model parameters is used (e.g., for the lack of a sufficient number of experimental measurements), which are not able to catch the most important dynamical and/or structural properties of the molecule. In our work we opted to abandon these phenomenological models in favor of a molecular description of relevant dynamics, i.e., the choice of important internal degrees of freedom described as usual generalized internal coordinates (bond lengths, bond angles, and torsion angles) to provide a clear physical description of the system giving the possibility to calculate a priori the molecular properties required in the parametrization of the stochastic model. This would also eliminate (or at least reduce to the minimum) the requirement of a fitting procedure.

Recently, a new approach has been presented by Wong et al.[9] in which a tentative step forward with respect to the phenomenological models has been done. It is substantially a Markovian states model,[10,11] where the molecule is thought to jump among a number of different rigid conformations, each of which can have a different global diffusion tensor. A diffusive equation is setup in which the global motion is treated as a diffusive motion and a master equation is introduced to describe the jumps between the different conformations. This model has been applied with success to the interpretation of NMR data of large biological molecules[12,13] in which slow conformational changes are observed. This kind of treatment is extremely interesting in the application to molecules showing slow large amplitude motions; however, it retains a phenomenological nature when also internal dynamics should be included (in particular the MF correlation function is used for the local dynamics). In this work we are presenting a model to describe in a "molecular" fashion those internal dynamics that are sufficiently slow so that their effect on NMR is not trivially a vibrational average but at the same time are not so slow and of large amplitude so that a strong collision operator is not suitable to describe them. Rather, in this case a continuous diffusive motion is more appropriate. Recently, we used this idea to define a simple stochastic model that was applied with success to the interpretation of both ESR[14,15] and NMR[3] spectroscopy data, in which the investigated molecules were described as flexible rotators with one internal diffusive torsional degree of freedom.

Integrated computational approaches have been developed by some of us for the calculation of both electron spin resonance (ESR)[2,16] and nuclear magnetic resonance (NMR)[3,4] spectroscopic observables of flexible molecules. The general protocol is based on the selection of suitable methods, of quantum mechanical (QM), classical (molecular mechanics, MM, and/or molecular dynamics, MD), and hydrodynamic (HD) nature, for the evaluation of molecular parameters. Parameters (free energy surfaces and dissipative tensors) are then fed into a Fokker–Planck (or Smoluchowski in the case of purely diffusive systems) equation for the evaluation of distribution probabilities or, directly, correlation functions and spectral densities; in some cases, this multiscale approach can be used in a predictive way. This approach of combining proper computational chemistry tools with a stochastic description of relevant molecular dynamics in terms of global tumbling coupled to important generalized internal coordinates (given in terms of lengths, angles and torsion angles) can be used to

dx.doi.org/10.1021/jp306627q | J. Phys. Chem. B 2012, 116, 14541–14555

describe a large number of different flexible biomolecules. The definition of the computational protocol for the complete parametrization and numerical solution of the resulting basic Smoluchowski equation is straightforward. Here we propose a generalized model adapted to the interpretation of NMR relaxation data which can be applied to flexible macromolecules ranging from small to medium oligosaccharides to, in principle, complex proteins. The model, called in the rest of this work simply the diffusive chain model (DCM) considers explicitly the global reorientation dynamics of the molecule together with the dynamics of a flexible body made of rigid units connected by joints, around which torsional motion is possible. The rigid units can be different in terms of size, shape, and chemical composition.

The numerically exact solution of the Smoluchowski equation becomes impracticable in terms of standard linear algebra matrix methods when more than three internal degrees of freedom need to be considered. This is associated to the exponential growth of the matrix dimensions. Two possible ways to solve the problem are (i) the introduction of approximate solution strategies, e.g., perturbative approaches based on the separability of time-scales, and (ii) the adoption of alternative formulations, formally equivalent to the original equations and amenable to less cost-expensive numerical approaches. In this paper we adopt the latter method by using an equivalent Langevin equation in which the high friction approximation is applied (see section II.C). The same ingredients entering the Smoluchowski equation, i.e., the diffusion tensor and the potential of mean force, are also parameters of the Langevin equation. Stochastic trajectories can be calculated easily such that statistical properties of the system (linked to the probability density) are correctly reproduced, using a standard Brownian dynamics (BD) approach.

We apply the DCM, both in its direct Smoluchowski form and in its BD implementation, to the interpretation of relevant dynamics of two case-studies of oligosaccharides, i.e., sugar units linked to form a linear chain, based on NMR relaxation data. The first case study is performed on the trisaccharide α-D-Man*p*-(1→2)-α-D-Man*p*-(1→6)-α-D-[6-^{13}C]-Man*p*-OMe, which will be labeled **TRI** in the following, represented in Figure 1a,b. In this case we employ a DCM model with two torsion angles (DCM_2), and therefore, a standard numerical solution of the Smoluchowski equation is adopted. This is done by spanning the diffusion operator over a set of basis functions and evaluating directly the correlation times affecting the NMR observables via matrix diagonalization. In the second case study we consider the pentasaccharide α-L-Fuc*p*-(1→2)-β-D-Gal*p*-(1→3)-β-D-Glc*p*NAc-(1→3)-β-D-Gal*p*-(1→4)-D-Glc*p*, **LNF-1**, depicted in Figure 1c,d. In this case four torsion angles are employed (DCM_4), and we use a BD numerical approach, by generating a number of stochastic trajectories and evaluating the correlation function by proper averaging. For this purpose we employ the BD_BOX software of Długosz et al.[17] Diffusion tensors are obtained via hydrodynamic methods for both molecules, while potential surfaces are obtained from unbiased molecular dynamics for **TRI** and from metadynamics[18] for **LNF-1**.

This paper is organized as follows: In section II some theoretical background is provided, and the stochastic model, its parametrization, and solution methods are discussed. In section III a description of the acquired experimental data is provided; Section IV is dedicated to the presentation and discussion of the results. Finally, in section V we give concluding remarks.

II. THEORETICAL AND COMPUTATIONAL BACKGROUND

In this section we provide a detailed description of the diffusive chain model, discussing the parametrization of the Smoluchowski time evolution equation and an overview of the standard numerical methods employed for solving it.

II.A. Modeling. As anticipated in the Introduction, the diffusive chain model associates the relevant dynamics of a flexible molecule to that of a linear or branched chain of rigid bodies linked by joints around which rotation is possible (torsion angles). A schematic representation of the model is provided in Figure 2. The stochastic process is $\mathbf{Q} = (\Omega,\boldsymbol{\theta})$,

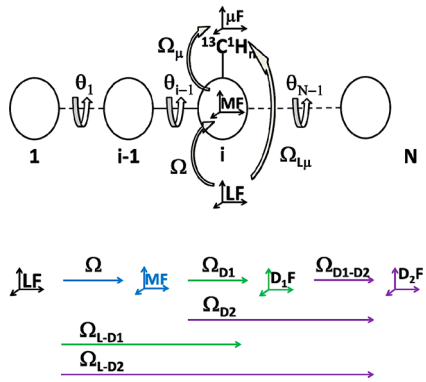

Figure 2. Schematic representation of the diffusive chain model (DCM). LF is the laboratory frame; MF is the molecular frame that diagonalizes the rotational part of the diffusion tensor placed on the reference body (*i* in the figure), which bears the spin probe; μF (μ = D1, D2 - dipolar frames) is the frame where the μth magnetic tensor is diagonal. Euler angles transforming among frames are defined. Transformations from LF to any other frame are time dependent; transformations among the other frames are time independent.

where Ω is the set of Euler angles transforming from the laboratory frame (LF) to a molecule-fixed frame (MF). The latter is chosen to be fixed on the body bearing the spin probe, and its orientation is such that the rotational part of the diffusion tensor of the molecule is diagonal. The array $\boldsymbol{\theta} = (\theta_1,...\theta_N)^{tr}$ includes all the N torsion angles taken into consideration in the model. In the diffusive regime the time dependence of the conditional probability density $P(\mathbf{Q},t|\mathbf{Q}_0,t_0)$ of finding the system in configuration $\mathbf{Q}$ at time t if it was in configuration $\mathbf{Q}_0$ at time t_0 is given by the diffusion or Smoluchowski equation[10]

$$\frac{\partial}{\partial t}P(\mathbf{Q}, t|\mathbf{Q}_0, t_0) = -\hat{\Gamma}(\mathbf{Q})P(\mathbf{Q}, t|\mathbf{Q}_0, t_0) \quad (1)$$

where the diffusive operator is defined as

$$\hat{\Gamma}(\mathbf{Q}) = -\begin{pmatrix}\hat{\mathbf{M}}\\ \frac{\partial}{\partial\boldsymbol{\theta}}\end{pmatrix}^{tr}\begin{bmatrix}\mathbf{D}_{RR}(\boldsymbol{\theta}) & \mathbf{D}_{RI}(\boldsymbol{\theta})\\ \mathbf{D}_{RI}^{tr}(\boldsymbol{\theta}) & \mathbf{D}_{II}(\boldsymbol{\theta})\end{bmatrix}P_{eq}(\mathbf{Q})\begin{pmatrix}\hat{\mathbf{M}}\\ \frac{\partial}{\partial\boldsymbol{\theta}}\end{pmatrix}P_{eq}^{-1}(\mathbf{Q}) \quad (2)$$

where $\hat{\mathbf{M}}$ is the infinitesimal rotation operator and $\partial/\partial\boldsymbol{\theta}$ is the gradient operator over all torsion angles. The full diffusion tensor of the system comprises the rotational part, $\mathbf{D}_{RR}(\boldsymbol{\theta})$, the internal part, $\mathbf{D}_{II}(\boldsymbol{\theta})$, and the rotational-internal mixed term,

dx.doi.org/10.1021/jp306627q | J. Phys. Chem. B 2012, 116, 14541−14555

$\mathbf{D}_{RI}(\boldsymbol{\theta})$. In eq 2 we show that these quantities are, in general, dependent on the molecular conformation, i.e., on the torsion angles. The equilibrium distribution appearing in the Smoluchowski equation is the canonical Boltzmann probability density

$$P_{eq}(\mathbf{Q}) = \exp[-V(\mathbf{Q})/k_BT]/\langle \exp[-V(\mathbf{Q})/k_BT]\rangle \quad (3)$$

where k_B is the Boltzmann constant, T is the temperature, and $V(\mathbf{Q})$ the potential of mean force (POMF) acting on the system. In the following the scaled potential $U = V/k_BT$ is used. The notation $\langle ...\rangle$ represents averaging over $\mathbf{Q}$.

To proceed, we need ways to estimate or evaluate the diffusion tensor and the POMF. The method for the calculation of the diffusion tensor is based on a HD approach, which is described at length in the literature.[19−22] Thus we provide here only a brief description. The molecule is modeled as an ensemble of N fragments (those building the diffusive chain), the ith fragment composed of N_i spheres (extended atoms), representing atoms or groups of atoms, and immersed in a homogeneous isotropic fluid of known viscosity. The full diffusion tensor, which is partitioned into translational (TT), rotational (RR), internal (II), and mixed parts (TR, TI, and RI) can be obtained from the inverse of the full friction tensor of the molecule, $\boldsymbol{\Xi}$, following Einstein's relation

$$\mathbf{D} = \begin{pmatrix} \mathbf{D}_{TT} & \mathbf{D}_{TR} & \mathbf{D}_{TI} \\ \mathbf{D}_{TR}^{tr} & \mathbf{D}_{RR} & \mathbf{D}_{RI} \\ \mathbf{D}_{TI}^{tr} & \mathbf{D}_{RI}^{tr} & \mathbf{D}_{II} \end{pmatrix} = k_BT\boldsymbol{\Xi}^{-1} \quad (4)$$

The full diffusion tensor of the molecule (constrained atoms) can be calculated starting from the unconstrained friction tensor, $\boldsymbol{\xi}$, of the free spheres and applying a geometric transformation depending upon the constraints. Details of the procedure are described elsewhere.[22] Notice that the free spheres friction tensor is defined in terms of the translational friction coefficient of a single sphere, given by Stokes's equation $\xi = CR\pi\eta$, as function of the temperature-dependent bulk viscosity η, the effective radius R and a constant C depending on boundary conditions.

Because we are interested in the interpretation of NMR relaxation data in a constant external magnetic field (i.e., no gradients) translations can be projected out. This results in the rotational-conformational motion and the diffusion tensor is represented by a $(3 + N_T) \times (3 + N_T)$ matrix (with $N_T = N - 1$ the number of torsion angles), partitioned in a purely rotational, purely internal and coupled roto-conformational terms, as was explicitly shown in eq 2. The full diffusion tensor depends on the molecular geometry, i.e., on the set of variables $\boldsymbol{\theta}$. This dependence is often rather weak, especially for relatively small molecules. In the following we will neglect the conformational dependence of the diffusion tensor in the case of **TRI**, while retaining it for the larger system **LNF-1**.

The second ingredient which is required is the POMF. We consider that the POMF does not depend on the global orientation of the molecule for isotropic systems, and therefore the equilibrium distribution depends only on the internal conformation, i.e., $P_{eq}(\mathbf{Q}) = P_{eq}(\boldsymbol{\theta})/8\pi^2$. An estimate of $P_{eq}(\boldsymbol{\theta})$ can be provided by unbiased or biased MD simulations, depending on the complexity of the system under study. In the case of unbiased MD the general approach is to recover the Boltzmann distribution probability $P_{eq}(\mathbf{Q})$ over the selected degrees of freedom $\mathbf{Q}$ by a histogram analysis of their time series and then recover the discrete (free energy) potential of mean force as $U(\mathbf{Q}) = -\ln(P_{eq}(\mathbf{Q})) + \text{const}$. The discrete representation of the surface is then fit with an appropriate analytical expression. In the case of biased trajectories, one can employ methods like metadynamics simulations,[18] adaptive biasing force calculations[23], or umbrella sampling.[24] In the case-studies considered in this work, we split the POMF as a sum of terms of two torsion angles only: $U(\boldsymbol{\theta}) = \sum_{i=1}^{N} U_j(\theta_i\theta_{i+1})$, with index i increasing by units of 2 and $j = \lfloor i/2 \rfloor$. We treat each pair of torsion angles separately and span the jth POMF term over the basis of complex exponentials

$$U_j(\theta_i, \theta_{i+1}) = \sum_{n_1=-\infty}^{\infty} \sum_{n_2=-\infty}^{\infty} u_{n_1n_2}^{(j)} \exp[-i(n_1\theta_1 + n_2\theta_2)] \quad (5)$$

Coefficients $u_{n_1n_2}^{(j)}$ are used to define the analytic expression of the POMF in eq 5, which can be plugged into the Smoluchowski operator (eq 2).

To summarize, we adopt the following steps for the modeling of the dynamics of a flexible molecule: (i) select the N_T relevant torsion angles to build the DCM_{NT}, namely a number of torsion (dihedral) angles defining the instantaneous internal geometry; (ii) evaluate the roto-conformational diffusive tensor via a HD approach; (iii) evaluate the POMF via averages taken over biased/unbiased MD trajectories. Once these steps are completed, one has the possibility to calculate NMR relaxation parameters (see below) of the system without the need of multicomponent fitting procedures, or with minimal fitting.

II.B. Evaluation of NMR Observables. We are interested here in molecules diffusing in low viscosity media such that molecular motions relax much faster than spin relaxation processes, i.e. we work fully within Redfield limit.[25] Following basic theory of spin relaxation[25] and making use of the theory of linear responses NMR relaxation data are evaluated directly from the spectral densities of the auto- and cross-correlation functions of magnetic interactions. Since for aliphatic $^{13}C^1H_n$ probes the CSA contribution can be neglected[26] only the dipolar terms enter the expressions of the relaxation data. In particular we are interested in the calculation of T_1, T_2, NOE, and the longitudinal and spin-lock dipolar cross-correlated relaxation rates (in the case of CH_2 probes). The explicit expressions are

$$\frac{1}{T_1} = \frac{b_{CH}^2}{10} \sum_{\mu} [J^{\mu,\mu}(\omega_H - \omega_C) + 3J^{\mu,\mu}(\omega_C) + 6J^{\mu,\mu}(\omega_H + \omega_C)] \quad (6)$$

$$\frac{1}{T_2} = \frac{b_{CH}^2}{20} \sum_{\mu} [4J^{\mu,\mu}(0) + J^{\mu,\mu}(\omega_H - \omega_C) + 3J^{\mu,\mu}(\omega_C) + 6J^{\mu,\mu}(\omega_H) + 6J^{\mu,\mu}(\omega_H + \omega_C)] \quad (7)$$

$$\text{NOE} = 1 + \frac{\gamma_H}{\gamma_C}\frac{b_{CH}^2}{10} T_1 \sum_{\mu} [6J^{\mu,\mu}(\omega_H + \omega_C) - J^{\mu,\mu}(\omega_H - \omega_C)] \quad (8)$$

$$\Gamma_{long} = \frac{3}{5} b_{CH}^2 J^{1,2}(\omega_C) \quad (9)$$

dx.doi.org/10.1021/jp306627q | J. Phys. Chem. B 2012, 116, 14541−14555

$$\Gamma_{\text{spin-lock}} = \frac{3}{10} b_{CH}{}^2 \left[\frac{4}{3} J^{1,2}(0) + J^{1,2}(\omega_C) \right] \tag{10}$$

where $J^{\mu,\nu}$ is the dipole−dipole auto- ($\mu = \nu$) or cross- ($\mu \neq \nu$) correlated spectral density, $b_{CH} = \mu_0 \gamma_H \gamma_C \hbar / 4\pi r_{CH}{}^3$, γ_X and ω_X are, respectively, the magnetogyric ratio and the Larmor frequency of nucleus X, and r_{CH} is the C−H bond length. The summation index in eqs 6−10 runs over the number of hydrogen nuclei bonded to the ^{13}C atom.

All spectral densities in the previous equations are obtained as Fourier−Laplace transforms of the normalized correlation functions

$$J^{\mu,\nu}(\omega) = \text{Re} \int_0^\infty \text{d}t e^{-i\omega t} \langle \mathcal{D}^J_{M,0}[\Omega_{L\mu}(0)]^* \mathcal{D}^J_{M,0}[\Omega_{L\nu}(t)] \rangle / \langle \mathcal{D}^J_{M,0}[\Omega_{L\mu}(0)]^* \mathcal{D}^J_{M,0}[\Omega_{L\nu}(0)] \rangle \tag{11}$$

where $\Omega_{L\mu}(t)$ is the stochastic set of Euler angles transforming from the laboratory frame, LF, to the principal axes frame of the μth magnetic tensor, μF, as shown in Figure 2. Equation 11 holds in the secular approximation. Because the magnetic interactions in which we are interested are represented by symmetric and traceless rank 2 tensors, only terms with $J = 2$ are preserved. Furthermore, due to the isotropy of the medium, we set $M = 0$. In eq 11 there is no explicit dependence on the torsional angles because, as stated above, we select MF being fixed on the body bearing the spin probe, which will be referred to as the reference body. The static purely geometric contribution of the magnetic part and the contribution of the dynamics of the system can be split in eq 11 by using the fact that $\Omega_{L\mu}(t) = \Omega_\mu + \Omega(t)$; that is, the orientation of the magnetic tensor with respect to LF is divided into the stochastic set of Euler angles, $\Omega(t)$, transforming from LF to MF, and a time-independent rotation over the reference body, Ω_μ, transforming from MF to μF (see Figure 2). Given this combined set of rotations and using the properties of Wigner matrices in eq 11, we obtain

$$\begin{aligned} J^{\mu,\nu}(\omega) &= 5 \sum_{K,K'=-2}^{2} \mathcal{D}^2_{K,0}(\Omega_\mu)^* \mathcal{D}^2_{K',0}(\Omega_\nu) \\ &\quad \text{Re} \int_0^\infty \text{d}t e^{-i\omega t} \langle \mathcal{D}^2_{0,K}[\Omega(0)]^* \mathcal{D}^2_{0,K'}[\Omega(t)] \rangle \\ &= 5 \sum_{K,K'=-2}^{2} \mathcal{D}^2_{K,0}(\Omega_\mu)^* \mathcal{D}^2_{K',0}(\Omega_\nu) j_{K,K'}(\omega) \end{aligned} \tag{12}$$

II.C. Solution Strategies. *Direct Evaluation of Spectral Densities.* In the case of **TRI**, we follow a standard method based on the projection of the diffusive operator on a proper set of basis functions. For the DCM we use the direct product basis set given

$$\begin{aligned} |\Lambda\rangle &= |\lambda\rangle \otimes |n_1\rangle \otimes \ldots \otimes |n_N\rangle \\ |\lambda\rangle &= |LMK\rangle = \sqrt{\frac{2L+1}{8\pi^2}} \mathcal{D}^L_{M,K}(\Omega) \\ |n_j\rangle &= \frac{1}{\sqrt{2\pi}} \exp(-i n_j \theta_j) \end{aligned} \tag{13}$$

Given the set of truncation parameters (L_{MAX}, $n_{1,MAX}$, ..., $n_{NT,MAX}$), all greater than or equal to zero, the number of basis functions N_b (and thus the matrix dimension) is in general $N_b = {}^1/_3(L_{MAX}+1)(2L_{MAX}+1)(2L_{MAX}+3)\Pi_{j=1}^{N_T}(2n_{j,MAX}+1)$. Due to the isotropy of the medium and the fact that we neglect nonsecular terms in the spin Hamiltonian, we can use symmetry arguments to fix $L = 2$ and $M = 0$, such that the matrix dimension reduced by symmetry is $N_b = 5\Pi_{j=1}^{N_T}(2n_{j,MAX}+1)$. Thus, as an example, in case of DCM_2 model for which $n_{1,MAX} = n_{2,MAX} = 40$ the number of basis functions is 32805.

Using the closure relation for the basis set $|\Lambda\rangle$ the reduced spectral densities can be rewritten in matrix form as

$$j_{K,K'}(\omega) = \mathbf{v}_K^{\text{tr}} (i\omega \mathbf{1} - \mathbf{\Gamma}) \mathbf{v}_{K'} \tag{14}$$

where $(\mathbf{\Gamma})_{i,j} = \langle \Lambda_i | \tilde{\Gamma} | \Lambda_j \rangle$ and $(\mathbf{v}_K)_i = \langle \Lambda_i | \mathcal{D}^2_{0,K}(\Omega) P_{\text{eq}}{}^{1/2} \rangle$; the symmetrized Hermitian form of the time evolution operator is employed

$$\tilde{\Gamma} = P_{\text{eq}}{}^{-1/2} \hat{\Gamma} P_{\text{eq}}{}^{1/2} \tag{15}$$

Details in the calculation of the matrix elements of the diffusive operator and projections of the physical observable over the basis functions are provided in Appendix A.

Introducing proper linear combinations of the Wigner matrices $\mathcal{D}^2_{0,K}(\Omega)$ it is possible to obtain a symmetrized version of eq 14, which allows implementing a simpler and optimized algorithm

$$j^S_{K,K'}(\omega) = \mathbf{v}^S_{K,K'} \cdot (i\omega \mathbf{1} - \mathbf{\Gamma})^{-1} \cdot \mathbf{v}^S_{K,K'} \tag{16}$$

where $\mathbf{v}^S_{K,K'}$ are linear combinations of $\mathbf{v}_K$ and $\mathbf{v}_{K'}$ arrays. Readers interested in mathematical and implementation details are referred to the basic papers on the methods.[3,7,27] To solve eq 16 we employ the Lanczos tridiagonalization[28,29] as described in paper 1.[30]

The whole procedure briefly discussed in this subsection is implemented in the C^{++}OPPS software package developed by some of us,[27,31] which is available to download under the GPL v2 license at the URL http://www.chimica.unipd.it/licc/software.html.

Brownian Dynamics. In the case of **LNF-1**, since the number of internal relevant degrees of freedom is significantly larger than the case of **TRI** molecule, we evaluate spectral densities from Brownian Dynamics trajectories.[32,33] We employ the software BD_BOX[17] to calculate directly stochastic trajectories by numerical integration of the equation

$$\dot{\mathbf{x}} = \mathbf{D}(\mathbf{x})[\mathbf{F}(\mathbf{x}) + \mathbf{R}(t)]/k_B T \tag{19}$$

where $\mathbf{x}$ is the array of beads positions, where each bead is an extended atom including hydrogen atoms and centered on carbon atoms. $\mathbf{R}$ is a white noise force such that $\langle R_j(t) \rangle = 0$, $\langle R_i(t) R_j(0) \rangle = \delta_{i,j} \rho_{i,j} \delta(t)$, i.e., forces are uncorrelated in time and among particles,[34] with the fluctuation−dissipation relation $\rho i_{,j} = 2k_B T \Xi_{i,j}$, where $\mathbf{D} = k_B T \mathbf{\Xi}^{-1}$. The diffusion tensor in eq 19 is in general a full matrix because hydrodynamic interactions among beads are taken into account employing the standard Rotne−Prager model.[35] This is done at the same level of approximation employed in the evaluation of the diffusion tensor in eq 4.

$\mathbf{F}$ is obtained from the gradient of the torsional potential term as defined in eq 5 plus constraining forces imposed to maintain rigid the structures of the sugar units. To create an efficient constraining of bond lengths and angles we impose strong harmonic potentials between triplets of beads, creating a triangular network of constraints among the atoms of the same sugar unit. Also, strong harmonic bending potentials can be used to avoid wobbling, with respect to the sugar units, of the

dx.doi.org/10.1021/jp306627q | J. Phys. Chem. B 2012, 116, 14541−14555

bonds around which torsion is possible. Naturally, a more direct approach would be based on an implementation of eq 19 considering internal and rotational coordinates (Ω,θ), but we have found that accurate and reliable trajectories are obtained using the simpler Cartesian representation, provided that time steps are kept small enough (see below).

Once trajectories are obtained, spectral densities are calculated from the correlation function of $\mathcal{D}^2_{0,0}(\Omega_{LD})$ defined for the set of Euler angles transforming from LF to the dipolar frame, DF. The latter is defined with the Z_D axis parallel to the C−H bond and the X_D and Y_D axes arbitrarily chosen (defining a right handed orthonormal set of axes) because of the axiality of the dipolar interaction. Because explicit hydrogen atoms are not calculated in the trajectory, the C−H normalized vector **v** is obtained from the sugar unit geometry and $\mathcal{D}^2_{0,0}(\Omega_{LD})$ is given by$(3v_z^2 - 1)/2$. Next, we can evaluate the autocorrelation function using a fast Fourier transform (FFT) method.[36,37] Finally, the spectral density is the real part of the Fourier transform of the correlation function.

To summarize, the following integrated protocol is adopted: we first perform full-atom deterministic metadynamics on selected relevant torsional angles to obtain a discrete representation of the potential of mean force. Next we obtain an analytical torsional potential from Fourier analysis which is employed, together with harmonic constraints, to calculate Brownian dynamics trajectories, with full treatment of fluctuation/dissipation including hydrodynamic interactions. Correlation functions and spectral densities are obtained from the stochastic trajectories.

III. EXPERIMENTAL SECTION

III.A. Trisaccharide. NMR experiments were performed on the trisaccharide α-D-Man*p*-(1→2)-α-D-Man*p*-(1→6)-α-D-[6-^{13}C]-Man*p*-OMe, the chemical synthesis of which will be described elsewhere, dissolved in a 7:3 molar ratio mixture of D_2O and DMSO-d_6 to a concentration of ∼18 mM. The solvents DMSO-d_6 and D_2O were obtained from Cambridge Isotope Laboratories, Inc. The solution was transferred to a 5-mm NMR tube and flame-sealed under vacuum after removing the dissolved gas by several cycles of ultrasonic bath and mild evacuation.

The experiments were carried out a temperature of 298 K at three magnetic fields. The experiments at 11.7 and 14.1 T were performed on Bruker Avance 500 and 600 spectrometers equipped with broadband (BBO) 5-mm probeheads, and the experiments at 16.4 T were performed on a Bruker Avance 700 spectrometer equipped with 5-mm TCI cryoprobe.

The sample temperature was calibrated carefully using the deuterated methanol chemical shift thermometer, whereas the temperature was regulated by means of the standard variable temperature controllers provided by the instrument manufacturers.

The carbon-13 spin−lattice relaxation time (T_1) was measured under decoupling using the standard inversion−recovery experiment with 12−16 variable delays between the inversion pulse and the read pulse. The number of scans was 256 at all magnetic fields, the recycle delay was ∼5 times longer than the longest T_1; four dummy scans were used to ensure steady-state conditions. Broadband proton decoupling during acquisition was performed using the Waltz-16 scheme, with typical decoupler 90° pulse duration of about 70 μs.

The spin−spin relaxation time (T_2) was measured using the standard CPMG spin−echo experiment using 12−16 different numbers of echoes. Constant echo time was used during the experiment, set to 0.4 ms at 11.7 T and 0.25 ms at 14.1 and 16.4 T. The number of scans was 512 at the two lower magnetic fields and 256 at highest magnetic fields. The recycle delay was set to ∼5 times T_1; 16 dummy scans were used.

The nuclear Overhauser enhancement (NOE) was measured using the dynamic NOE experiment with reduced decoupling power during the NOE buildup time. Two experiments with long (>5 T_1) and short (1 ms) irradiation were recorded; enhancement factors were obtained as a ratio between peak intensities of the two experiments. The recycle delay was longer than 10 times T_1; four dummy scans were used. The number of scans was 512 for the two lower magnetic fields and 256 for the highest magnetic field.

The nuclear relaxation rates associated with cross-correlated dipole−dipole interactions were measured according to the protocol described by Ghalebani et al.[38] We measured longitudinal dipole−dipole cross-correlated relaxation rates (CCRRs) using the carbon-13 inversion−recovery experiment without decoupling. Relaxation rates of the lines of the *J*-coupled triplet were analyzed separately using the initial rates approach and CCRRs were obtained as the difference between individual rates. Relaxation delays for the inversion−recovery sequence were chosen in the range from 100 μs to 50 ms (less than half of the typical T_1 in order to ensure the initial rate regime) and one or two long delays were included to provide the reference spectra. The number of scans was set to 1024 at the two lower fields (11.7 and 14.1 T) and to 512 at the highest field (16.4 T).

Prior to the Fourier transformation of all FIDs, a line broadening of 1−5 Hz was applied. The nonlinear fitting routines provided by the instrument manufacturers were used for evaluating the T_1 and T_2 relaxation times and CCRRs. The carbon-13 90° pulse was 7 μs at 11.7 T, 12 μs at 14.1 T, and 7.95 μs at 16.4 T. The spectral width was typically set to 100 ppm; the carrier frequency was set close to resonance (∼65 ppm). The accuracy of T_1, T_2, NOE, and CCRR data is estimated to be better than 3%, 5%, 5%, and 10%, respectively. All experiments were carried out 2−3 times, and average values are reported.

III.B. LNF-1. NMR spectra on the same **LNF-1** sample as used previously[39,40] were recorded at 30 °C on a Bruker AVANCE III 600 MHz spectrometer (14.09 T) equipped with a 5 mm BBO probe (one T_2 experiment) and a Bruker AVANCE III 700 MHz spectrometer (16.44 T) equipped with a 5 mm TCI Z-Gradient Cryoprobe (5 T_1, 4 T_2, and 8 HetNOE experiments) using the experimental procedures described earlier.[39] Data processing was performed using vendor-supplied software. The standard deviations for all 16.44 T data were <1.5%.

IV. RESULTS

IV.A. Trisaccharide. We first analyze results concerning the trisaccharide **TRI**, schematically depicted in Figure 1a. Internal torsion angles are labeled $\theta = (\omega,\psi_2)$, with ω = O5−C5−C6−O6 and ψ_2 = C1″−O2′−C2′−H2′ (for atoms numbering see Figure 1b).

A 300 ns explicit solvent molecular dynamics simulation of the trisaccharide was carried out using the force field recently developed by MacKerell and co-workers.[41] The simulation revealed significant flexibility in the linkages between the

dx.doi.org/10.1021/jp306627q | J. Phys. Chem. B 2012, 116, 14541−14555

Table 1. MD Simulation Parameters for the Trisaccharide

force field	CHARMM36 all-atom hexopyranoses (year 2009)
software	CHARMM c35b4
molecular charge	0
number of water molecules	2167
water molecule model	TIP3P
cubic periodic box dimension	40.391 × 40.391 × 40.391 Å^3
ensemble	N (6570), P (1 atm), T (298 K)
thermostat	Nosé-Hoover (tmass 7910 kcal mol^{-1} ps^{-2})
barostat	Nosé-Hoover Langevin (pmass 791 amu, pgamma 20 ps^{-1}, tbath 298 K)
nonbonded interactions cutoff	12 Å, smoothing switch at 10 Å
pair list distance	14 Å
electrostatics	PME (κ 0.35, order 6, 36 Å)
time step of integration	2 fs
coordinates saving frequency	1000 MD steps
equilibration period	200 ps
production period	300 ns

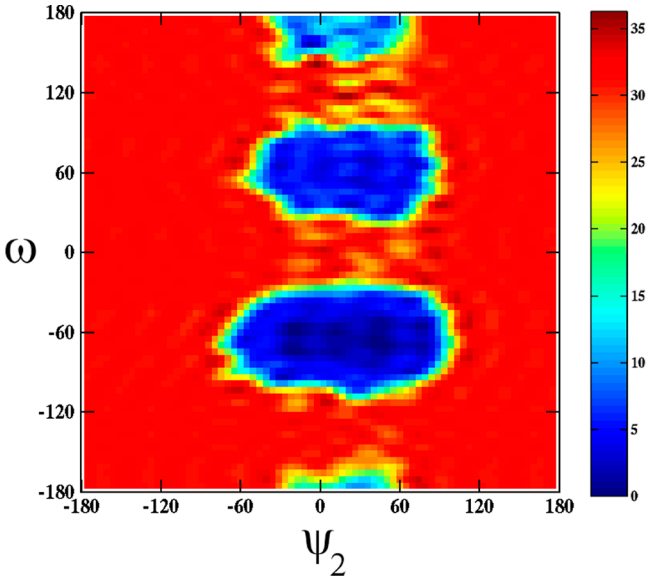

Figure 3. Potential of mean force obtained from the analysis of the unbiased MD trajectory of the ω and ψ_2 torsion angles of the **TRI** molecule. The potential is given in k_BT units at T = 298 K.

carbohydrate residues. Parameters of the simulation are given in Table 1. The trajectory was produced with the CHARMM c35b4[42] software package. For the-(1→2)-linkage, one finds that the ϕ-torsion (H1″-C1″-O2′-C2′) maintains the *exo*-anomeric conformation with an average value of −43° while the ψ-torsion is in a rapid equilibrium between two states centered at +40° and −15°, populated in a 2:1 ratio. The α-(1→6)-linkage is found to be essentially in a single state with ϕ = −52° (H1′-C1′−O6-C6), ψ = 174° (C1′−O6−C6-C5) and ω = −60°. Although the populations of the nonsubstituted hydroxymethyl groups are in excellent agreement with those derived from $^3J_{H5,H6pro\text{-}R}$ and $^3J_{H5,H6pro\text{-}S}$ coupling constants,[43] the homonuclear coupling constants in the reducing end residue suggest that the ω torsion of the (1→6)-linkage exists as a mixture of the *g*+ (+65°), *g*− (−65°), and *t* (180°) states in a ratio of 45:47:8, respectively. Based on these results, it is concluded that the ω- and ψ_2-torsion angles are the most important ones.

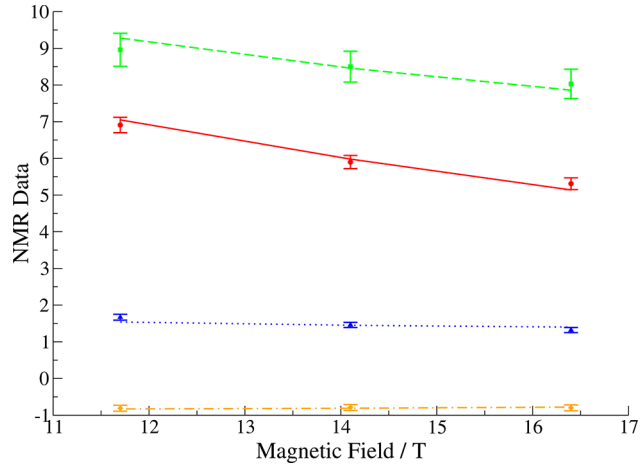

Figure 4. Calculated (lines) and experimental (points) NMR data of **TRI** as function of the magnetic field: R_1 (red line/circles) in s^{-1}, R_2 (green dashed line/squares) in s^{-1}, NOE (blue dotted line/triangles), and Γ_{long} (orange dash-dotted line/diamonds) in s^{-1}.

Table 2. MD Simulation Parameters for the Metadynamics Simulations of the Pentasaccharide

force field	CSFF
software	NAMD
molecular charge	0
number of water molecules	699
water molecule model	TIP3P
cuboid periodic box dimension	31.432 × 31.808 × 27.492 Å^3
ensemble	N (2210 atoms), P (1 atm), T (300 K)
thermostat	temperature coupling
barostat	Nosé − Hoover Langevin piston (piston period 200 fs, piston decay 100 fs, piston temperature 300 K)
nonbonded interactions cutoff	12 Å, smoothing switch at 10 Å
pair list distance	13.5 Å
electrostatics	PME (κ 0.35, order 6, 32 Å)
time step of integration	2 fs
coordinates saving frequency	250 MD steps
equilibration period	1 ns
unbiased MD period	200 ns
metadynamics	50 ns, hillWidth 2.

The potential of the mean force can be obtained directly from the unbiased molecular dynamics trajectories. The potential surface is depicted in Figure 3, based on the histogram analysis of the trajectory of the two torsional angles. The length of the trajectory was tested to be sufficient to catch the equilibrium properties of the torsion angles by comparing the energy surface calculated at different times. Just after 150 ns the POMF showed to be stable with respect to trajectory length (see Supporting Materials for more details).

Dissipative properties, i.e., the elements of the diffusion tensor **D**, were evaluated using the software DITE,[14] which

dx.doi.org/10.1021/jp306627q | J. Phys. Chem. B 2012, 116, 14541−14555

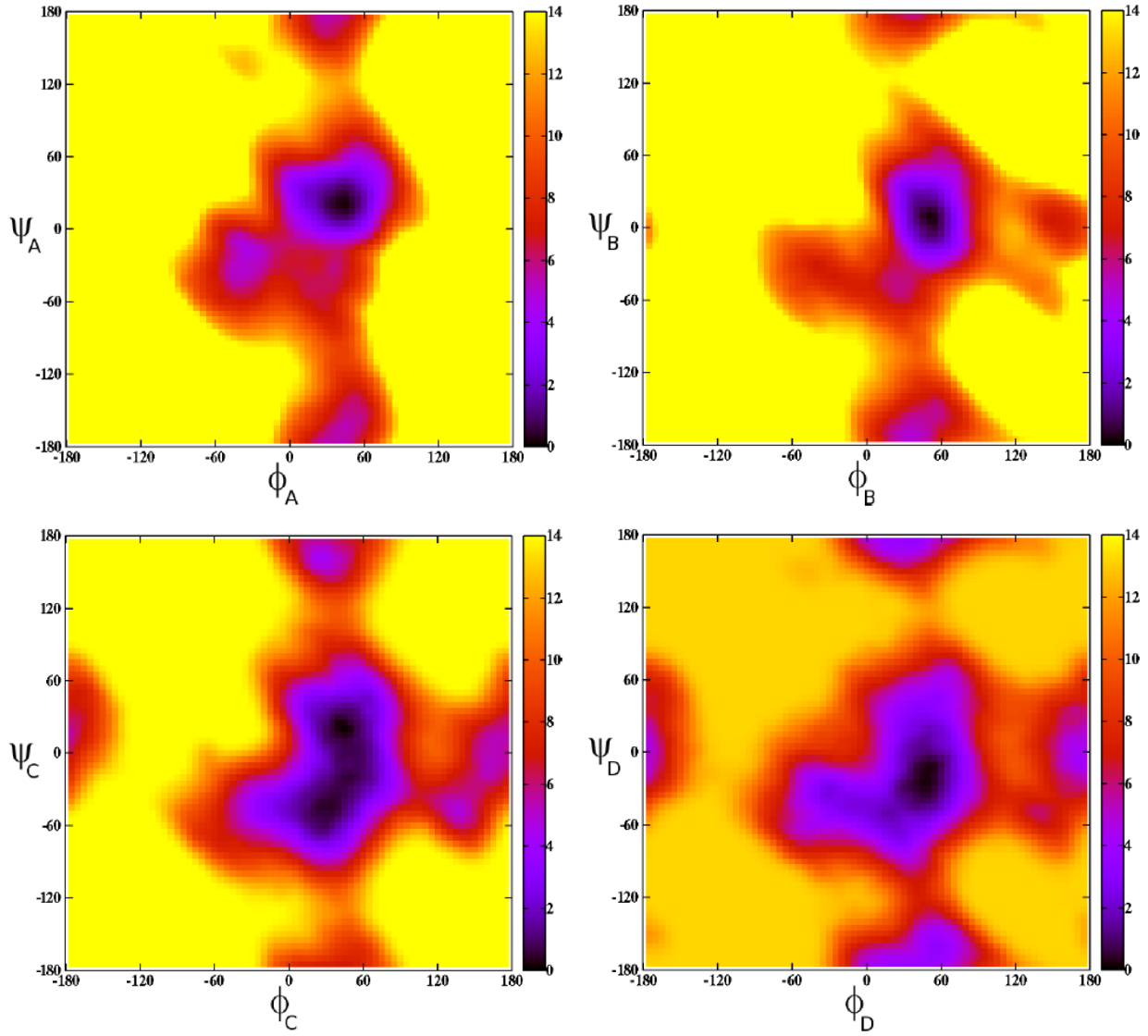

Figure 5. Potential of mean force surfaces for the four couples of torsion angles connecting **LNF-1** sugar units obtained from metadynamics simulations. The potential is given in k_BT units at T = 300 K.

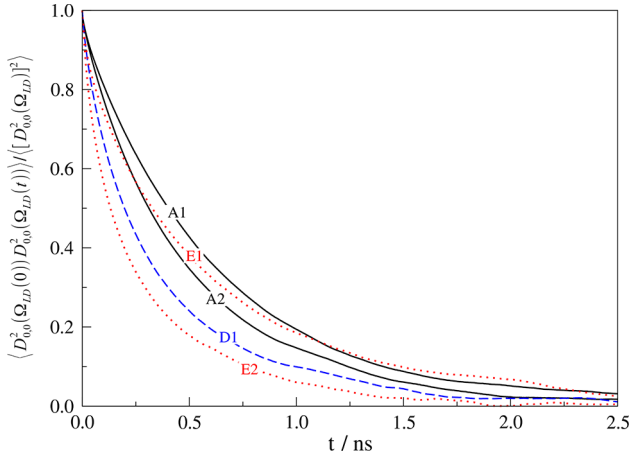

Figure 6. Selected autocorrelation functions of $\mathcal{D}^2_{0,0}(\Omega_{LD})$ for $^{13}C^1H$ probes A1 and A2 (solid black line) in ring A, D1 (dashed blue line) in ring D, and E1 and E2 (dashed red line) in ring E_α of the **LNF-1** molecule obtained from Brownian dynamics simulations.

implements the HD approach presented in section II.A. The full diffusion tensor was calculated at T = 298 K, viscosity of the water-DMSO solution η = 3.66 cP,[44] with stick boundary conditions (C = 6) and effective radius of spheres R = 2.0 Å. In the simulations of **TRI** NMR data, we assumed a configuration-independent diffusion tensor, calculated in the absolute minimum energy geometry (with respect to the ω and ψ_2 angles). This approximation is justified by considering that (i) the larger contribution to NMR relaxation will be provided by geometry fluctuations around the absolute energy minimum (the other two minima are located at about 3 k_BT and 6 k_BT over the absolute minimum) and (ii) the observation that the diffusion tensor is practically independent of the ω angle and variation on ψ_2 around the minimum energy is limited to ±10%. Good agreement with experimental data (see below) confirmed that this apparently strong approximation is sufficient to catch the most important dissipative properties of the system to reproduce NMR relaxation data.

We simulated relaxation data of the $^{13}C^1H_2$ probe highlighted in Figure 1b at 298 K and ^1H frequencies of 500, 600, and 700 MHz, using two free parameters, namely a multiplicative

dx.doi.org/10.1021/jp306627q | J. Phys. Chem. B 2012, 116, 14541−14555

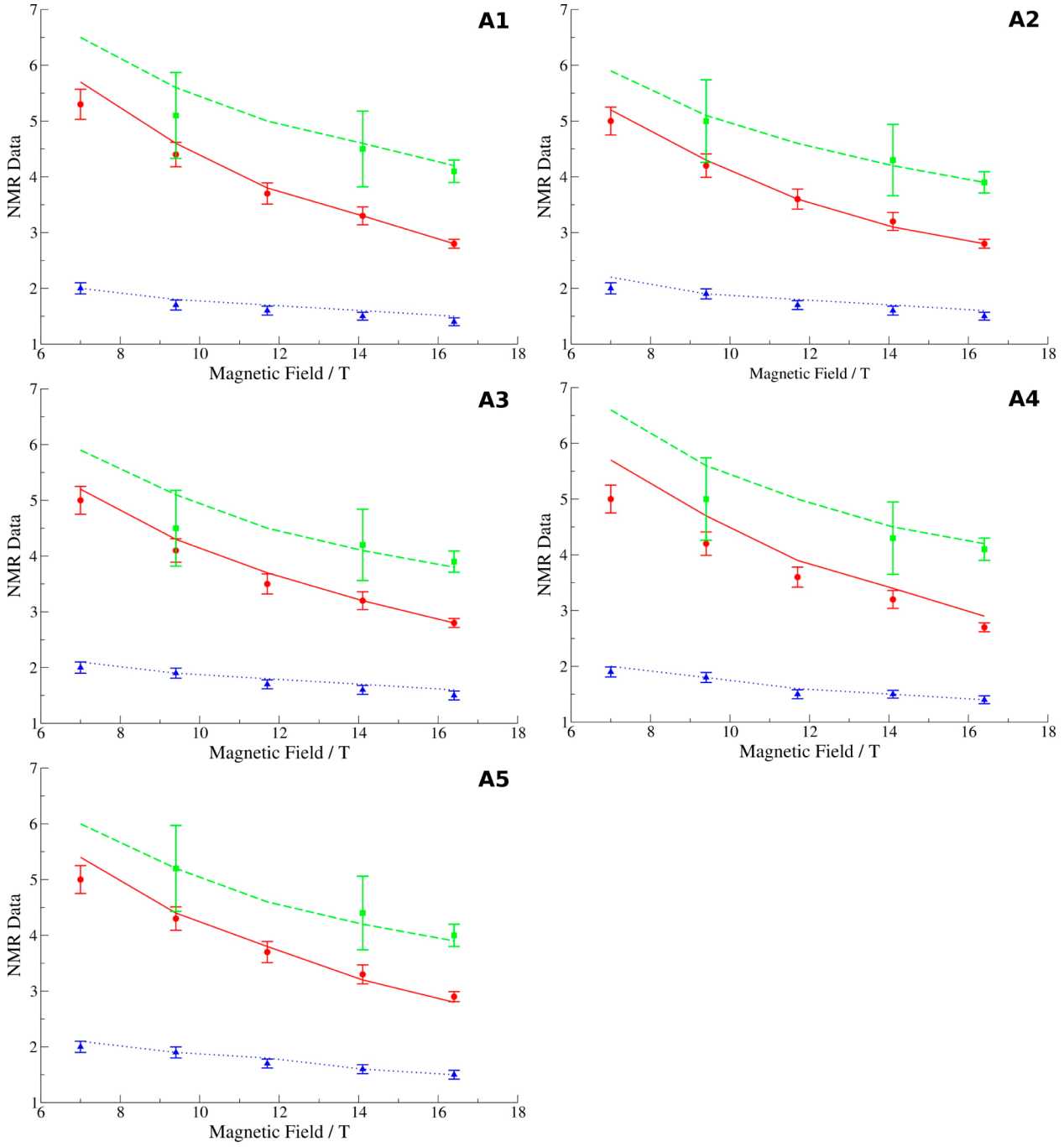

Figure 7. Calculated (lines) and experimental (points) NMR data of **LNF-1** A ring as function of the magnetic field: R_1 (red line/circles) in s^{-1}, R_2 (green dashed line/squares) in s^{-1}, and NOE (blue dotted line/triangles).

constant of the diffusion tensor, d, and the H−C−H angle, α_{H-C-H}, to which the cross-correlated dipolar relaxation rates are sensitive. The C−H bond length was set to 1.13 Å.[45,46] Results are depicted in Figure 4, and both experimental and theoretical data are reported in Table S3 of the Supporting Information. The reduced χ^2 is equal to 1.247; the estimated correction of the diffusion tensor is d = 0.6 and α_{H-C-H} = 116.3°. A 0.6 scaling of the diffusion tensor is a reasonable correction that takes into account both experimental deviations from the medium viscosity and/or temperature, and corrections to the RC product, which constitutes the effective adjustable parameter of the HD model for the diffusion tensor.

The H−C−H shows a 6% deviation from the tetrahedral angle, 109.5°, with an estimation uncertainty ±1° for a ±10% error in CCRR rates. This discrepancy has been observed for other similar systems[3,47,48] and indicate the effect of internal motion,[38,46] as proofed also in Appendix B of paper 1.[30]

IV.B. LNF-1. A 200 ns long MD simulation of **LNF-1** was carried out using NAMD[49] with the parameters shown in Table 2, after energy minimization, heating, and equilibration at 300 K. The NAMD software was employed due to its better performance in terms of computation time and thus more suitable for a larger molecule. In the simulations, the CSFF[50] force field was used for the **LNF-1** molecule. This trajectory can be used to inspect the energetic profile of the system and

dx.doi.org/10.1021/jp306627q | J. Phys. Chem. B 2012, 116, 14541−14555

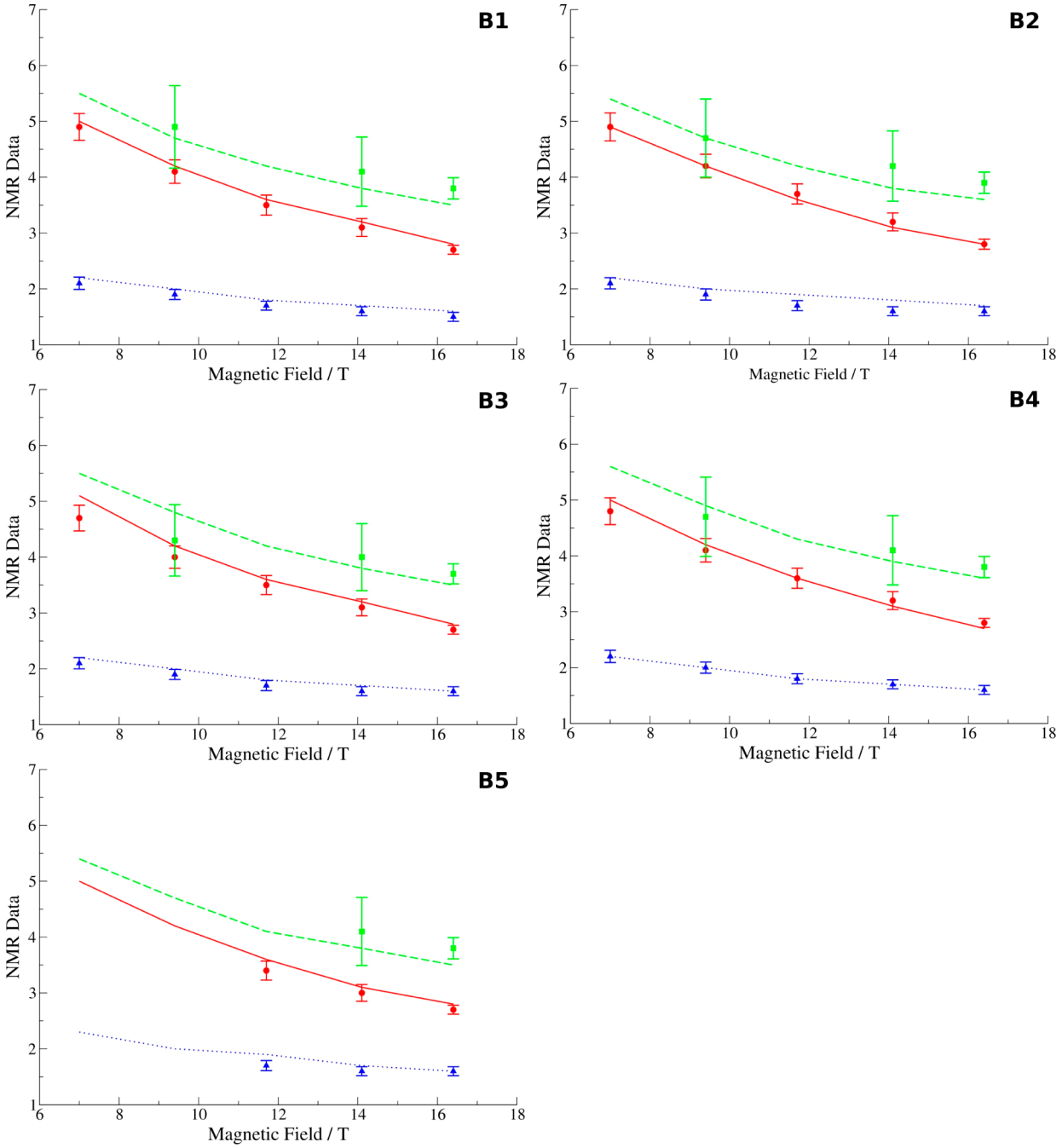

Figure 8. Calculated (lines) and experimental (points) NMR data of **LNF-1** B ring as function of the magnetic field: R_1 (red line/circles) in s^{-1}, R_2 (green dashed line/squares) in s^{-1}, and NOE (blue dotted line/triangles).

decide, heuristically, which degrees of freedom are relevant. We consider the four couples of (ϕ,ψ) torsional angles among sugar units, i.e., $\boldsymbol{\theta} = (\phi_A,\psi_A,\phi_B,\psi_B,\phi_C,\psi_C,\phi_D,\psi_D)$, where the terminal atoms in each torsion are a hydrogen atom and a carbon atom. Average values of dihedral angles over the trajectory are in agreement with previously published results:[40] $(\phi_A,\psi_A) = (41.8°,22.4°)$, $(\phi_B,\psi_B) = (49.8°,9.3°)$, $(\phi_C,\psi_C) = (41.6°,-5.2°)$, and $(\phi_D,\psi_D) = (45.0°,-4.1°)$. This is taken as reference structure in further calculations.

To simplify the representation of the internal potential, we assume that it can be split in approximately four terms, as anticipated in section II.A, each depending on one of the couples of torsional angles, i.e.

$$U(\boldsymbol{\theta}) = \sum_{i=A,B,C,D} U_i(\phi_i, \psi_i) \tag{20}$$

We evaluated the four terms separately in four different metadynamics simulations. Parameters are reported in Table 3. In Figure 5 we report the plots of the four terms. It can be seen that the couples of angles (ϕ_A,ψ_A) and (ϕ_B,ψ_B) are confined within deep potential wells around the average values of the torsion angles, while the potential surfaces for the (ϕ_C,ψ_C) and (ϕ_D,ψ_D) couples of angles show a broader distribution. Also, relaxation times of the A and B couples of angles are much smaller than those for the other angles (see the Supporting Information). On the basis of these observations, we assume that angles (ϕ_A,ψ_A) and (ϕ_B,ψ_B) are subjected to fast librational

dx.doi.org/10.1021/jp306627q | J. Phys. Chem. B 2012, 116, 14541−14555

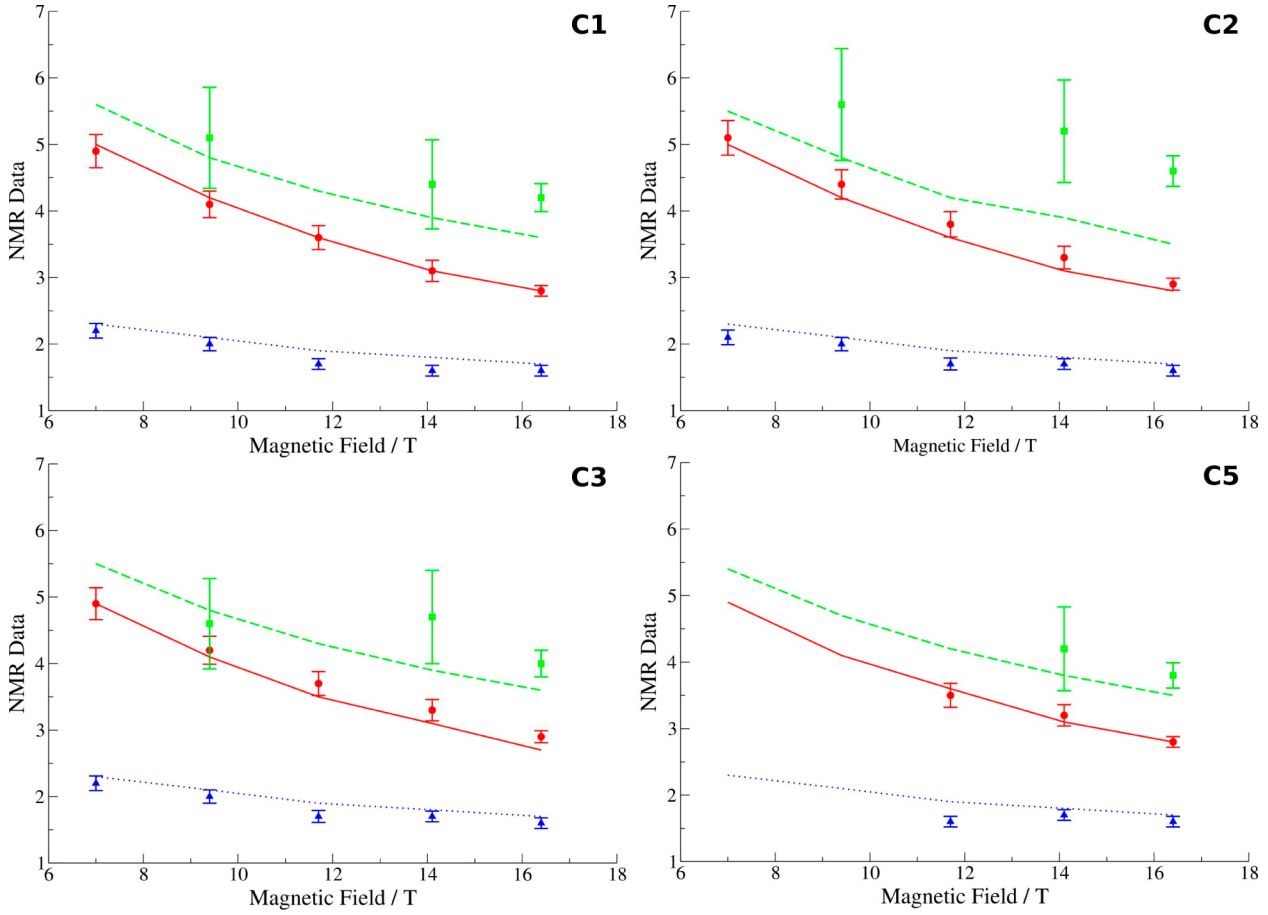

Figure 9. Calculated (lines) and experimental (points) NMR data of **LNF-1** C ring as function of the magnetic field: R_1 (red line/circles) in s^{-1}, R_2 (green dashed line/squares) in s^{-1}, and NOE (blue dotted line/triangles).

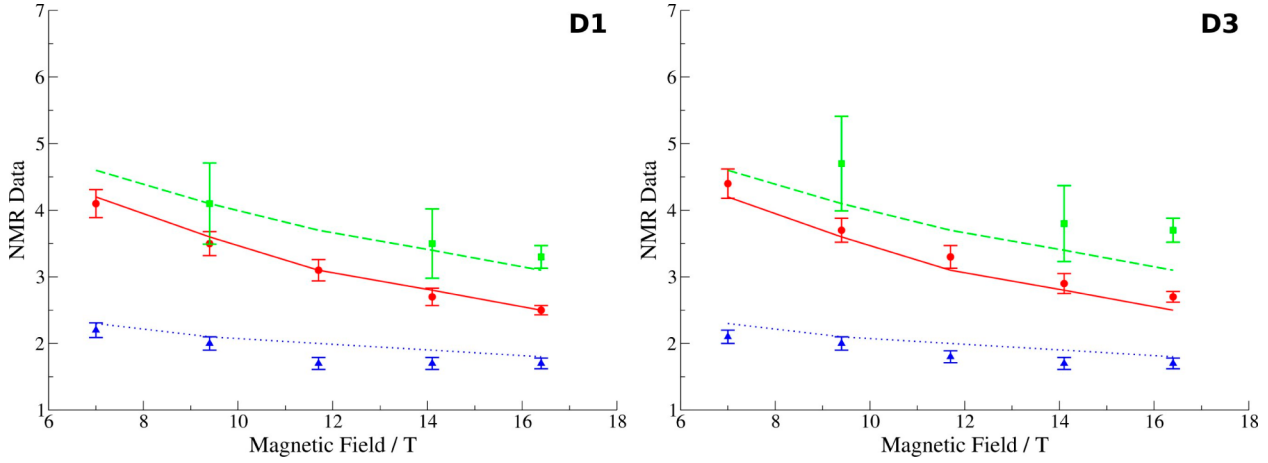

Figure 10. Calculated (lines) and experimental (points) NMR data of **LNF-1** D ring as function of the magnetic field: R_1 (red line/circles) in s^{-1}, R_2 (green dashed line/squares) in s^{-1}, and NOE (blue dotted line/triangles).

motions around minimum values, to which they are approximated. Thus, the relevant internal coordinates are limited to $\boldsymbol{\theta} = (\phi_C,\psi_C,\phi_D,\psi_D)$, as depicted in Figure 1c. It is clear that neglecting the (ϕ_A,ψ_A) and (ϕ_B,ψ_B) angles may have an effect on the quality of the simulated NMR data. However, we conjecture that this contribution is small compared to the other angles and the choice of the relevant coordinates $(\phi_C,\psi_C,\phi_D,\psi_D)$ is sufficient to reach a good agreement between simulated and experimental data keeping a simpler (and faster in terms of computational time) description of the system. Good comparison with experimental data provide a feedback on the correctness of our assumption.

Following the integrated scheme described above, the torsional potential energy, interpolated as a Fourier expansion, was employed to calculate Brownian dynamics trajectories. Only the internal angles $\boldsymbol{\theta} = (\phi_C,\psi_C,\phi_D,\psi_D)$ were allowed to change, whereas the rest of the molecule was assumed to be rigid. This means that in case of **LNF-1** three groups of atoms

dx.doi.org/10.1021/jp306627q | J. Phys. Chem. B 2012, 116, 14541−14555

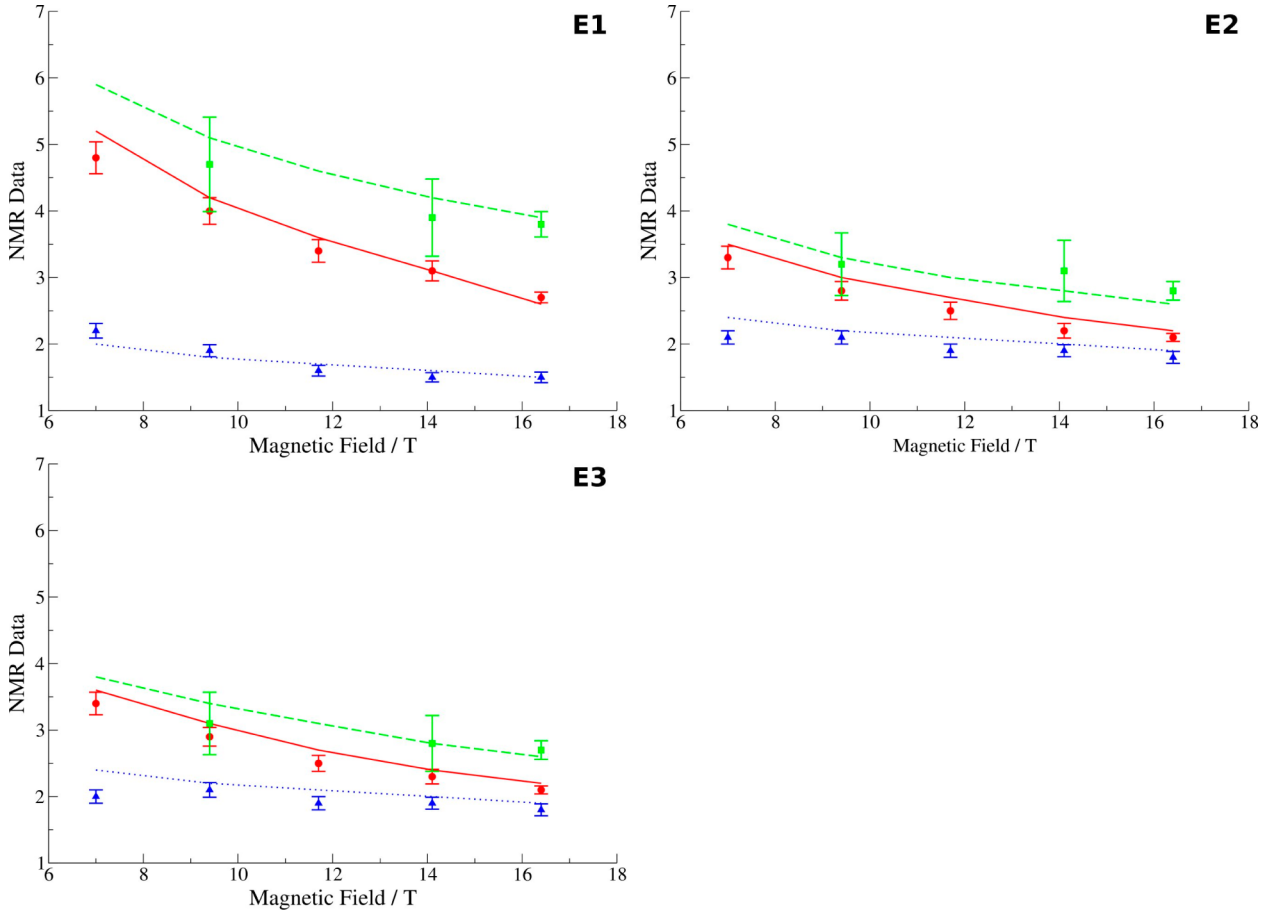

Figure 11. Calculated (lines) and experimental (points) NMR data of **LNF-1** E_α ring as function of the magnetic field: R_1 (red line/circles) in s^{-1}, R_2 (green dashed line/squares) in s^{-1}, and NOE (blue dotted line/triangles).

have to be constrained, i.e., the group of the three sugar units A, B, and C; unit D; and unit E. In accordance with previous work[3] the hydrodynamic radius of each bead was set to 2 Å. Other simulation parameters were: temperature equal to 303 K, viscosity to 1.4 cP.[44] The integration time step was chosen to be δt = 10 fs, with data snapshots saved every 200 integration steps, i.e., 2 ps. Correlation functions and spectral densities were calculated from a 1.5 μs Brownian dynamics trajectory.

We show in Figure 6 some correlation functions for selected carbon atoms. We note that carbons 1 and 2 of the A ring have a clearly different relaxation behavior, which is related to the relative orientation of the two C−H vectors with respect to the molecular frame. This difference, reflected in a different set of NMR data for the two carbon atoms, can be attributed to the anisotropic reorientation of the **LNF-1** molecule which differentiates the relaxation behavior of carbons with axial and equatorial hydrogen atoms in the ring A.[39] The autocorrelation function of carbon 1 in the D ring decays noticeably faster, and carbon 2 of the E ring has the fastest decay, whereas interestingly, carbon 1 of the E ring behaves like carbon atoms of the A ring. This is due to the spatial position of the corresponding C−H vector, which makes it quite insensitive to the internal motions of the D and E rings.

For the calculation of the NMR relaxation parameters a C−H bond length of r_{CH} = 1.13 Å was used.[45,46] The overall comparison of the resulting calculated parameters with the experimental ones is shown in Figures 7−11. Experimental and theoretical data are fully reported in Tables S4−S8 of the Supporting Information. The agreement between theoretical and experimental values is adequate, with most differences within ±10%, which can be considered satisfactory since no adjustable parameters were used. Some larger disagreements are observed for the T_2 values for the C2 carbon (Figure 9), which may perhaps be due to the conformational exchange of the N-acetyl group linked to this carbon.[40,51] NOE values are consistently 5−10% higher than experimental values. This can be a sign of a slightly too fast motion due to a not sufficiently accurate evaluation of dissipative properties. This in turn can be associated to hydrodynamic parameters (the need of increasing the beads radii) or to some disagreement between the real experimental bulk properties of the solution, i.e., temperature and viscosity, and those used in the calculation of dissipative properties.

V. CONCLUSIONS

The diffusive chain model presented in this work provides a general framework to describe coupled global-internal relevant dynamics, with respect to NMR observables, of flexible molecules whose internal mobility is mainly of torsional nature. This approach can, in principle, be applied to several biomolecules, from small to medium oligosaccharides, used as case studies in this paper, to (in principle) proteins. The model, associated to a computational protocol to evaluate the potential of mean force and the full diffusion tensor, can provide, at a relatively modest computational cost, a coherent and quantitatively adequate agreement of simulated relaxation

dx.doi.org/10.1021/jp306627q | J. Phys. Chem. B 2012, 116, 14541−14555

times with experimental ones. The choice of the internal relevant degrees of freedom remains a general conundrum, which however in this work has been approached using chemical insight and knowledge acquired from previous works on similar systems.

It is clear that our approach is (still) not applicable to large biomolecules, as large proteins, DNA, etc., showing large amplitude motions because it would require the solution of the Smoluchowski equation over hundreds of internal coordinates, if one does not accounts also for the difficulty of recovering Boltzmann distributions, even if methods based on non-equilibrium transformations seem to be promising on this matter.[52] One point of strength of our model and approach, however, is that it is possible to calculate all the molecular parameters a priori, as it was shown specially for the case of the LNF-1 molecule, where no fitting parameters were used. We believe that a hybrid approach in which slow, large amplitude motions are treated with the Wong et al.[9] model and the local "faster" motions are modeled with our approach may constitute an important advancement in the modeling of relevant dynamics of complex systems.

APPENDIX A: MATRIX ELEMENTS OF THE DCM DIFFUSIVE OPERATOR

In this appendix we provide the details for the calculation of matrix elements of the Smoluchowski operator defined in eq 2 and projections of the starting vector on the orthonormal basis given in eq 13. These are needed to evaluate quantities given in eq 15 to be used in the calculation of the symmetrized reduced spectral densities defined in eq 16.

The DCM diffusive operator can be split, for convenience, into three terms

$$\hat{\Gamma}_{RR} = \hat{\mathbf{J}}^{tr}\mathbf{D}_{RR}(\boldsymbol{\theta})P_{eq}(\mathbf{Q})\hat{\mathbf{J}}P_{eq}{}^{-1}(\mathbf{Q})$$

$$(1+\delta_{jk})\hat{\Gamma}_{jk} = -\frac{\partial}{\partial\theta_j}D_{jk}P_{eq}(\mathbf{Q})\frac{\partial}{\partial\theta_k}P_{eq}{}^{-1}(\mathbf{Q}) - \frac{\partial}{\partial\theta_k}D_{jk}P_{eq}(\mathbf{Q})\frac{\partial}{\partial\theta_j}P_{eq}{}^{-1}(\mathbf{Q})$$

$$\hat{\Gamma}_{Rj} = -i\hat{\mathbf{J}}^{tr}\mathbf{D}_{Rj}P_{eq}(\mathbf{Q})\frac{\partial}{\partial\theta_j}P_{eq}{}^{-1}(\mathbf{Q}) - i\frac{\partial}{\partial\theta_j}\mathbf{D}_{Rj}^{tr}P_{eq}(\mathbf{Q})\hat{\mathbf{J}}P_{eq}{}^{-1}(\mathbf{Q}) \quad (A1)$$

We are interested in the case of isotropic medium, thus we can set $P_{eq}(\mathbf{Q}) = P_{eq}(\boldsymbol{\theta})/8\pi^2$. Moreover, we are making the approximation that the diffusion tensor is independent of molecular geometry, i.e., $\mathbf{D}(\boldsymbol{\theta}) \approx \mathbf{D}$. Within these assumptions, the three terms of the diffusive operator, in symmetrized form, become

$$\tilde{\Gamma}_{RR} = \hat{\mathbf{J}}^{tr}\mathbf{D}_{RR}\hat{\mathbf{J}}$$

$$(1+\delta_{jk})\tilde{\Gamma}_{jk} = -2D_{jk}\frac{\partial^2}{\partial\theta_j\partial\theta_k} - \frac{1}{2}D_{jk}\left[\frac{\partial U(\boldsymbol{\theta})}{\partial\theta_j}\frac{\partial U(\boldsymbol{\theta})}{\partial\theta_k} - 2\frac{\partial^2 U(\boldsymbol{\theta})}{\partial\theta_j\partial\theta_k}\right]$$

$$\tilde{\Gamma}_{Rj} = 2i\sum_{\alpha=+,-,z}D_\alpha^{(\alpha)}\hat{J}_\alpha\frac{\partial}{\partial\theta_j} \quad (A2)$$

where $2D_{Rj}^{(\pm)} = D_{Rj}^{(x)} \mp D_{Rj}^{(y)}$ and $\hat{J}_\pm = \hat{J}_x \pm i\hat{J}_y$.

So we need to evaluate the following matrix elements

$$\langle\Lambda|\tilde{\Gamma}|\Lambda'\rangle = \delta_n\langle\lambda|\tilde{\Gamma}_{RR}|\lambda'\rangle + \sum_j\delta_{\bar{n}_j}(\delta_{\lambda,\lambda'}\langle n_j|\tilde{\Gamma}_{jj}|n_j'\rangle + \delta_{L,L'}\delta_{M,M'}\langle K, n_j|\tilde{\Gamma}_{Rj}|K', n_j'\rangle) + \sum_{k>j}\delta_{\lambda,\lambda'}\delta_{\bar{n}_j,n_k}\langle n_j, n_k|\tilde{\Gamma}_{jk}|n_j', n_k'\rangle \quad (A3)$$

where $\delta_n = \Pi_j\,\delta_{nj,nj'}$ $\delta_{\bar{n}_j} = \Pi_{k\neq j}\,\delta_{nk,nk'}$, and $\delta_{\bar{n}_j,n_k} = \Pi_{l\neq j,k}\,\delta_{nl,nl'}$.

The potential of mean force is written in the form $U(\boldsymbol{\theta}) = -\Sigma_{v=(v_1,\ldots v_N)}\chi_v|v\rangle$ where $|v\rangle = |v_1\rangle\ldots|v_N\rangle = \exp[-i(v_1\theta_1 + \ldots v_1\theta_1)]/(2\pi)^{N/2}$. Derivatives are evaluated straightforwardly

$$\frac{\partial U(\boldsymbol{\theta})}{\partial\theta_j} = i\sum_v\chi_v v_j|v\rangle$$

$$\frac{\partial U(\boldsymbol{\theta})}{\partial\theta_j}\frac{\partial U(\boldsymbol{\theta})}{\partial\theta_k} = -\sum_{v,v'}\chi_v\chi_{v'}v_jv_k'|v\oplus v'\rangle$$

$$\frac{\partial^2 U(\boldsymbol{\theta})}{\partial\theta_j\partial\theta_k} = \sum_v\chi_v v_jv_k|v\rangle \quad (A4)$$

where $|v\oplus v'\rangle = |v_1 + v_1'\rangle\ldots|v_N + v_N'\rangle$. It follows that

$$\langle\lambda|\tilde{\Gamma}_{RR}|\lambda'\rangle = \delta_{L,L'}\delta_{M,M'}\Bigg\{\delta_{K,K'}\left[D_{RR}^{(z)}K^2 + \frac{D_{RR}^{(+)}}{4}(c_{L,K}^{+,2} + c_{L,K}^{-,2})\right] + \frac{D_{RR}^{(-)}}{4}(\delta_{K,K'+2}c_{L,K-2}^{+}c_{L,K-1}^{+} + \delta_{K,K'-2}c_{L,K+1}^{+}c_{L,K+2}^{+})\Bigg\}$$

$$\langle n_j|\tilde{\Gamma}_{jj}|n_j'\rangle = \delta_{n_j,n_j'}D_{jj}n_j^2 - \frac{D_{jj}}{4}\sum_{v\oplus v'=n\oplus(-n')}\chi_v v_j(\chi_{v'}v_j' + 2\delta_{v',0}v_j)$$

$$\langle K, n_j|\tilde{\Gamma}_{Rj}|K', n_j'\rangle = -2\delta_{n_j,n_j'}n_j[\delta_{K,K'-1}D_{Rj}^{(-)}c_{L,K+1}^{-} + \delta_{K,K'}D_{Rj}^{(Z)}K + \delta_{K,K'+1}D_{Rj}^{(+)}c_{L,K-1}^{+}]$$

$$\langle n_j, n|\tilde{\Gamma}_{jj}|n_j', n_k'\rangle = 2\delta_{n_j,n_j'}\delta_{n_k,n_k'}D_{jk}n_jn_k - \frac{D_{jk}}{2}\sum_{v\oplus v'=n\oplus(-n')}\chi_v v_j(\chi_{v'}v_k' + 2\delta_{v',0}v_k) \quad (A5)$$

where $D_{RR}^{(\pm)} = D_{RR}^{(xx)} \pm D_{RR}^{(yy)}$, $c_{LK}^{\pm} = (L(L+1) - K(K\pm1))^{1/2}$, and $2D_{Rj}^{(\pm)} = D_{Rj}^{(x)} \mp D_{Rj}^{(y)}$, while the compact notations $\Sigma_{v\oplus v'=n\oplus(-n')} = \Sigma_{v1+v1'=n1-n1'}\Sigma_{v2+v2'=n2-n2'}\ \ldots\ \Sigma_{vN+vN'=nN-nN'}$ and $\delta_{v,0} = \Pi_j\delta_{vj,0}$.

It is convenient, from a computational point of view, to transform the basis in such a way that the matrix associated to the diffusive operator is real. To this purpose we define the new basis set

dx.doi.org/10.1021/jp306627q | J. Phys. Chem. B 2012, 116, 14541−14555

$$|\Lambda\rangle_{K,n} = [2(1 + \delta_{K,0}\delta_{n,0})]^{-1/2} e^{-i\pi(j-1)/4}(|+\rangle + js|-\rangle) \tag{A6}$$

where $s = (-1)^{L+K}$, $\delta = \Pi j\delta_{nj,0}$, $|\pm\rangle = |L,M,\pm K,\pm n\rangle$, and indexes J, K and n ranges are

$$\begin{cases} K=0 & n_1=0 & n_2=0 & \dots & n_N=0 & j=(-)^L \\ K=0 & n_1=0 & n_2=0 & \dots & n_N>0 & j=\pm 1 \\ \vdots & \vdots & \vdots & \vdots & \vdots & \vdots \\ K=0 & n_1=0 & n_2>0 & \dots & |n_N|\le n_N^{\max} & j=\pm 1 \\ K=0 & n_1=0 & |n_2|\le n_2^{\max} & \dots & |n_N|\le n_N^{\max} & j=\pm 1 \\ K>0 & |n_1|\le n_1^{\max} & |n_2|\le n_2^{\max} & \dots & |n_N|\le n_N^{\max} & j=\pm 1 \end{cases} \tag{A7}$$

The matrix elements of the Smoluchowski operator in the new basis set, $\{|\Lambda\rangle_{K,n}\}$, can be written as functions of the matrix elements of the starting basis set, $\{|\Lambda\rangle\}$, as

$$\langle\Lambda|\tilde{\Gamma}|\Lambda'\rangle = N_{\Lambda,\Lambda'}[\delta_{j,j'}\mathrm{Re}(\langle+|\tilde{\Gamma}|+\rangle + j's'\langle+|\tilde{\Gamma}|-\rangle) + j\delta_{j,-j'}\mathrm{Im}(\langle+|\tilde{\Gamma}|+\rangle + j's'\langle+|\tilde{\Gamma}|-\rangle)] \tag{A8}$$

where $N_{\Lambda,\Lambda'} = 2[2(1 + \delta_{K,0}\delta_{n,0})]^{1/2}[2(1 + \delta_{K',0}\delta_{n',0})]^{1/2}$.

Finally we write the expression for the projections of the observable on the basis (starting vector). The program C^{++}OPPS employs a set of functions, $T^{\pm}_{k,k'}$, expressed as linear combinations of $\mathcal{D}^2_{0,k}(\Omega)$ (see refs 21 and 24 for details), where Ω is the set of Euler angles from the laboratory frame, LF, to the molecule-fixed frame, MF, which diagonalizes the rotational diffusion tensor, and is fixed over the fragment bearing the spin probe. The projection of the basis functions over these functions is

$$\langle\Lambda|T^{(\pm)}_{k,k'}\rangle \propto \sqrt{[L]}\,[2(1 + \delta_{K,0}\delta_{n,0})]^{1/2}\delta_{L,2}\,\delta_{M,0}[\delta_{K,k} \pm (-)^K\delta_{K,-k'} + \delta_{K,k'} \pm (-)^K\delta_{K,-k'}] \times(\pm\delta_{j,\pm 1}\mathrm{Re}\langle n|P_{\mathrm{eq}}(\boldsymbol{\theta})\rangle + \delta_{j,\pm 1}\mathrm{Im}\langle n|P_{\mathrm{eq}}(\boldsymbol{\theta})\rangle) \tag{A9}$$

where $\langle n|P^{1/2}_{\mathrm{eq}}(\theta)\rangle \propto \int_0^{2\pi} d\theta_1 \dots \int_0^{2\pi} d\theta_N \exp(i\Sigma_j n_j\theta_j) P^{1/2}_{\mathrm{eq}}(\theta)$ can be evaluated numerically.

■ ASSOCIATED CONTENT

Supporting Information

Both experimental and theoretical data. This material is available free of charge via the Internet at http://pubs.acs.org.

■ AUTHOR INFORMATION

Corresponding Author

*E-mail: antonino.polimeno@unipd.it. Phone: (+39) 049 8275146. Fax: (+39) 049 8275829.

Notes

The authors declare no competing financial interest.

■ ACKNOWLEDGMENTS

This work was supported by Ministero dell'Istruzione, Università e Ricerca (MIUR), grant PRIN Time 2008, by the University of Padova, grant "Progetto Strategico" Helios 2009, and by the CMST COST Action CM1002 "CODECS". Support from the Swedish Research Council (contracts 621-2010-4890 and 621-2011-3311) and The Knut and Alice Wallenberg Foundation is gratefully acknowledged. Computing resources were kindly provided by the Center for Parallel Computers (PDC), Stockholm, Sweden. The work was also supported by the grant SVV-2012-265305 from the Czech ministry of education.

■ REFERENCES

(1) Barone, V.; Polimeno, A. *Chem. Soc. Rev.* **2007**, *36*, 1724.
(2) Barone, V.; Polimeno, A. *Phys. Chem. Chem. Phys.* **2006**, *8*, 4609.
(3) Zerbetto, M.; Polimeno, A.; Kotsyubynskyy, D.; Ghalebani, L.; Kowalewski, J.; Meirovitch, E.; Olsson, U.; Widmalm, G. *J. Chem. Phys.* **2009**, *131*, 234501.
(4) Zerbetto, M.; Buck, M.; Meirovitch, E.; Polimeno, A. *J. Phys. Chem. B* **2011**, *115*, 376.
(5) (a) Lipari, G.; Szabo, A. *J. Am. Chem. Soc.* **1982**, *104*, 4546. (b) Lipari, G.; Szabo, A. *J. Am. Chem. Soc.* **1982**, *104*, 4559.
(6) Polimeno, A.; Freed, J. H. *Adv. Chem. Phys.* **1993**, *83*, 89.
(7) Polimeno, A.; Freed, J. H. *J. Phys. Chem.* **1995**, *99*, 10995.
(8) Meirovitch, E.; Shapiro, Y. E.; Polimeno, A.; Freed, J. H. *J. Phys. Chem. A* **2006**, *110*, 8366.
(9) Wong, V.; Case, D. A.; Szabo, A. *Proc. Natl. Acad. Sci. U.S.A.* **2009**, *106*, 11016.
(10) (a) Swope, W. C.; Pitera, J. W.; Suits, F. *J. Phys. Chem. B* **2004**, *108*, 6571. (b) Swope, W. C.; Pitera, J. W.; Suits, F.; Pitman, M.; Eleftheriou, M.; Fitch, B. G.; Germain, R. S.; Rayshubski, A.; Ward, T. J. C.; Zhestkov, Y.; Zhou, R. *J. Phys. Chem. B* **2004**, *108*, 6582.
(11) Singhal, N.; Snow, C. D.; Pande, V. S. *J. Chem. Phys.* **2004**, *121*, 415.
(12) Ryabov, Y.; Clore, G. M.; Schwieters, C. D. *J. Chem. Phys.* **2012**, *136*, 034108.
(13) Ermani, P. S.; Olsen, G. L.; Varani, G.; Drobny, G. P. *J. Phys. Chem. A* **2011**, *115*, 12055.
(14) Zerbetto, M.; Polimeno, A.; Cimino, P.; Barone, V. *J. Chem. Phys.* **2008**, *2008*, 24501.
(15) Hermosilla, L.; Sieiro, C.; Calle, P.; Zerbetto, M.; Polimeno, A. *J. Phys. Chem. B* **2008**, *112*, 11202.
(16) Zerbetto, M.; Polimeno, A.; Barone, V. *Com. Phys. Com* **2009**, *180*, 2680.
(17) Długosz, M.; Zielinski, P.; Trylska, J. *J. Comput. Chem.* **2011**, *32*, 2734.
(18) Laio, A.; Parrinello, M. *Proc. Natl. Acad. Sci. U.S.A.* **2002**, *99*, 12562.
(19) (a) Bloomfield, V. A.; Dalton., W. G.; Van Holde, K. E. *Biopolymers* **1967**, *5*, 135. (b) Bloomfield, V. A. *Science* **1968**, *161*, 1212.
(20) Moro, G. *Chem. Phys.* **1987**, *118*, 181.
(21) (a) De La Torre, J. G.; Bloomfield, V. A. *Rev. Biophys.* **1981**, *14*, 81. (b) De La Torre, J. G.; Huertas, M. L.; Carrasco, B. *J. Magn. Reson.* **2000**, *147*, 138.
(22) Barone, V.; Zerbetto, M.; Polimeno, A. *J. Comput. Chem.* **2009**, *30*, 2.
(23) Darve, E.; Pohorille, A. *J. Chem. Phys.* **2001**, *115*, 9169.
(24) Kumar, S.; Rosenberg, J. M.; Bouzida, D.; Swendsen, R. H.; Kollman, P. A. *J. Comput. Chem.* **1992**, *13*, 1011.
(25) Abragam, A. *The Principles of Nuclear Magnetism*; Oxford University Press (Clarendon): Oxford, 1961.
(26) Chen, Y. Y.; Luo, S. Y.; Hung, S. C.; Chan, S. I.; Tzou, D. L. M. *Carbohydr. Res.* **2005**, *340*, 723.
(27) Zerbetto, M.; Polimeno, A.; Meirovitch, E. *J. Phys. Chem. B* **2009**, *113*, 13613.
(28) Moro, G. J.; Freed, J. H. *J. Chem. Phys.* **1981**, *74*, 3757.
(29) Moro, G. J.; Freed, J. H. *Large-Scale Eigenvalue Problems, Math Studies Series*; Cullum, J., Willough, R., Eds.; North Holland: Amsterdam, 1986; Vol. *127*, p 143.
(30) Zerbetto, M.; Kotsyubynskyy, D.; Kowalewski, J.; Widmalm, G.; Polimeno, A. *J. Phys. Chem. B* **2012**, *116*, 13159.
(31) Zerbetto, M.; Polimeno, A.; Meirovitch, E. *Int. J. Quantum Chem.* **2010**, *110*, 387.

(32) Gillepsie, D. T. *Am. J. Phys.* **1993**, *61*, 1077.
(33) Gardiner, C. W. *Handbook of stochastic methods: for physics, chemistry and the natural sciences*; Springer: Berlin, Germany, 2004.
(34) Risken, H. *The Fokker-Planck Equation: Methods of Solution and Applications*; Springer: Berlin, Germany, 1992.
(35) Rotne, J.; Prager, S. *J. Chem. Phys.* **1969**, *50*, 4831.
(36) Allen, M. P.; Tildesley, D. J. *Computer Simulation of Liquids*; Clarendon Press Oxford Science Publications: Oxford, U.K., 1987.
(37) Box, G. E. P.; Jenkins, G. M.; Reinsel, G. C. *in Time Series Analysis: Forecasting and Control*, 3rd ed.; Prentice-Hall: Upper Saddle River, NJ, 1994.
(38) Ghalebani, L.; Bernatowicz, P.; Nikkhou Aski, S.; Kowalewski, J. *Concepts Magn. Reson* **2007**, *30*, 100.
(39) Rundlöf, T.; Venable, R. M.; Pastor, R. W.; Kowalewski, J.; Widmalm, G. *J. Am. Chem. Soc.* **1999**, *121*, 11847.
(40) Säwén, E.; Stevensson, B.; Östervall, J.; Maliniak, A.; Widmalm, G. *J. Phys. Chem. B* **2011**, *115*, 7109.
(41) Guvench, O.; Hatcher, E.; Venable, R. M.; Pastor, R. W.; MacKerell, A. D., Jr. *J. Chem. Theory Comput.* **2009**, *5*, 2353.
(42) Brooks, B. R.; Bruccoleri, R. E.; Olafson, B. D.; States, D. J.; Swaminathan, S.; Karplus, M. *J. Comput. Chem.* **1983**, *4*, 187.
(43) Stenutz, R.; Carmichael, I.; Widmalm, G.; Serianni, A. S. *J. Org. Chem.* **2002**, *67*, 949.
(44) Schichman, S. A.; Amey, R. L. *J. Phys. Chem.* **1971**, *75*, 98.
(45) Henry, E. R.; Szabo, A. *J. Chem. Phys.* **1985**, *82*, 4753.
(46) Kowalewski, J.; Effemey, M.; Jokisaari, J. *J. Magn. Reson.* **2002**, *157*, 171.
(47) Ghalebani, L.; Kotsyubynskyy, D.; Kowalewski, J. *J. Magn. Reson.* **2008**, *195*, 1.
(48) Kövér, K. E.; Batta, G.; Kowalewski, J.; Ghalebani, L.; Kruk, D. *J. Magn. Reson.* **2004**, *167*, 263.
(49) Phillips, J. C.; Braun, R.; Wang, W.; Gumbart, J.; Tajkhorshid, E.; Villa, E.; Chipot, C.; Skeel, R. D.; Kale, L.; Schulten., K. *J. Comput. Chem.* **2005**, *26*, 1781.
(50) Kuttel, M.; Brady, J. W.; Naidoo, K. J. *J. Comput. Chem.* **2002**, *23*, 1236.
(51) Zaccheus, M.; Pendrill, R.; Jackson, T. A.; Wang, A.; Auzanneau, F.-I.; Widmalm, G. *Eur. J. Org. Chem.* **2012**, *25*, 4075.
(52) Vaikuntanathan, S.; Jarzynski, C. *J. Chem. Phys.* **2011**, *134*, 054107.